RSC Advances

ROYAL SOCIETY OF CHEMISTRY

www.rsc.org/advances

After a threshold doping level of Mn, it is possible to alter from two photon absorption to saturable absorption in ZnO nanorods.

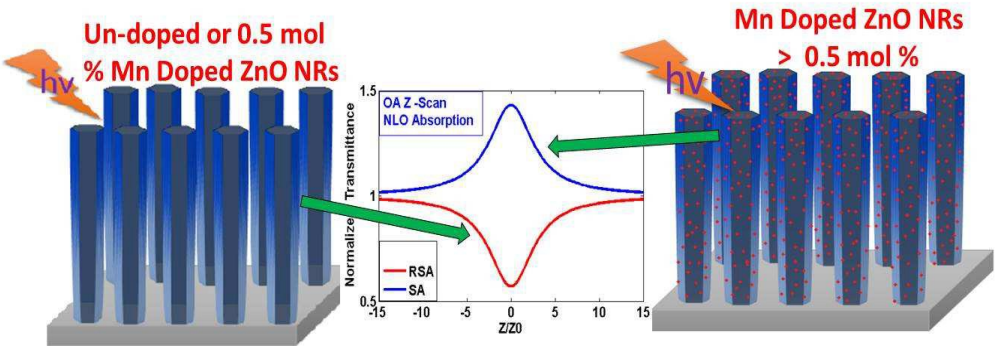

Journal Name

ARTICLE

Defect-assisted saturable absorption characteristics in Mn doped ZnO Nano-rods

Received 00th January 20xx,
Accepted 00th January 20xx

DOI: 10.1039/x0xx00000x

www.rsc.org/

Avanendra Singh[1], Samir Kumar[1], Ritwick Das, and Pratap K. Sahoo[*]

We have investigated the manifestations due to Manganese (Mn)-doping in ZnO sub-wavelength rods (or nanorods) on its nonlinear optical properties, namely two-photon absorption (TPA) and nonlinear refraction using single-beam Z–scan technique. Mn-doped ZnO nanorods (NRs) were prepared by low temperature aqueous growth technique. The results show that Mn-doping concentration primarily determines whether ZnO NRs would exhibit saturable absorption (SA) or two-photon-absorption (TPA) characteristics in an open-aperture experiment. At high Mn-doping concentrations, ZnO NRs exhibit SA behaviour which could be attributed to high occupation probability of defects states as well as saturation of linear absorption of sub-wavelength rod aggregates at high optical fluence. In contrast to high Mn-doping concentration in ZnO NRs, we observed TPA feature in 0.5% Mn-doped ZnO NRs. The employability of such structures in the area of optical limiting and switching is essentially derived from the possibility to tune the nonlinear optical absorption which could be realized by appropriate Mn-doping in ZnO NR architecture.

[1] *A. Singh and S. Kumar contributed equally to this work.*
*School of Physical Sciences, National Institute of Science Education and Research (NISER) Bhubaneswar, Odisha, India-751005,*avanendra.s@niser.ac.in, samir.kumar@niser.ac.in, *ritwick.das@niser.ac.in , pratap.sahoo@niser.ac.in*

**Corresponding author: pratap.sahoo@niser.ac.in, phone: +91-674-2304042*

† Footnotes relating to the title and/or authors should appear here.
Electronic Supplementary Information (ESI) available: [details of any supplementary information available should be included here]. See DOI: 10.1039/x0xx00000x

Introduction

Amongst many semiconductor materials, ZnO has received considerable attention in the area of nonlinear optics primarily due to its great potential for a variety of applications.[1] In comparison to bulk, ZnO-based sub-wavelength structures exhibit enhanced optical nonlinearities and fast response time as a consequence of material as well as structural resonance effects.[2,3] For example, one-dimensional (1D) ZnO sub-wavelength sized crystals or nanocrystals exhibit a wide range of promising applications in UV photonic devices,[4] field emission devices,[5,6] sensors,[7] and piezoelectric nanogenerators.[8] It is worthwhile to note that ZnO is a wide band gap (3.4eV) semiconductor which can be grown into subwavelength structures varying in size from a few tens of nanometer to a few hundred nanometer using physical as well as chemical methods. However, the recipe adopted to grow such ZnO based aggregates primarily determines their physical and chemical properties.[1] This happens due to different surface morphology and varying spatial arrangement of ZnO subwavelength clusters. For example, optical confinement of aligned ZnO-nanorods (NRs) arrays results into improved optical emission properties which could be useful in UV lasing along the long-axis of aligned NRs.[9,10] Due to unequal atomic dimensions of Zn as well as O along with high inherent polar potentials of ZnO crystal,[11,12]ZnO exhibits enhanced optical nonlinearity. The nonlinear optical processes such as second-harmonic-generation (SHG) and self-phase modulation (SPM) etc. exhibit remarkable enhancement by virtue of resonant transitions to exciton levels in ZnO NRs as well as in ZnO thin films.[13]

It is worthwhile to note that doping in ZnO can significantly tune the bandgap which can be employed for favorably altering optical as well as electronic properties of sub-wavelength aggregates.[14,15] For example, it was observed that the spintronic properties of ZnO films could be enhanced through Mn, Co, Ni, or Fe doping as a consequence of strong coupling of magnetic moments of dopants in the aggregates of host (ZnO).However the structural and physical properties of such aggregates must be thoroughly understood to use as devices operating at or above room temperature.[16,17]Among all magnetic ion-doped ZnO architectures, Mn-doping has received considerable attention essentially due to high thermal solubility and excellent lattice-matching with ZnO matrix.[18] It is to be noted that Mn is an isovalent impurity for Zn, and the ionic radius (0.066 nm) of Mn^{2+} is comparable to that of Zn^{2+} (0.060 nm) which results in a theoretical solubility limit of 35% for Mn, while maintaining the wurtzite structure of ZnO thin films.[2,19] Also, it has been proposed that the observation of room-temperature ferromagnetism in Mn-doped ZnO thin films could be due to the stabilization of an oxygen-deficient Mn_xO_y secondary phase which results in an exchange interaction between magnetic moments localized at Mn sites mediated by free charge carriers.[20] It is interesting to note that this ferromagnetic ordering results in magnetization-induced modifications in nonlinear optical susceptibilities ($\chi^{(2)}_{ijk}$, $\chi^{(3)}_{ijkl}$ etc.) which results in enhanced efficiencies for second-harmonic-generation (SHG), self-focusing/defocusing four-wave mixing etc.[21] Therefore, it is expected that the nonlinear optical (NLO) properties of Mn-doping in ZnO based sub-wavelength aggregates could substantially differ from bulk ZnO or thin-films essentially due to additional electric-dipole contribution from geometrical effects as well as magnetization-induced effects. However, a comprehensive investigation of third-order nonlinear optical properties of Mn-doped ZnO based sub-wavelength architectures is yet to be carried out for ascertaining the role of geometry as well as magnetization (due to Mn-doping). In this work, we present a detailed study on nonlinear refractive-index (NLR) and two photon absorption (TPA) coefficient for different fractions of Mn-doping in ZnO nanorods which have been fabricated using hydrothermal chemical wet synthesis at low temperature.[22] The NLO behaviour of NRs was ascertained using single-beam Z-scan technique with frequency doubled mode-locked Nd: YVO4 laser pulses in sub-nanosecond regime.[23]

Experimental Details

Commercially available 500 nm thick sputter coated indium tin oxide (ITO) layer were used as substrates for ZnO NR growth. Analytical grade zinc nitrate and hexamethylenetetramine (HMTA) were obtained from Sigma Aldrich. The substrates were ultrasonically cleaned in acetone, ethanol and de-ionized (DI) water for 10 minutes each. Subsequently, the substrates were cleaned in freshly prepared aquaregia (3HCl+HNO3) for 5 minutes in an

ultrasonic bath followed by thorough rinsing in DI water. The cleaned substrates were vertically immersed in an aqueous solution of 0.5M Zinc Nitrate hexahydrate, 0.5M HMTA and 0.5%, 1.5%, 2.0%, 2.5% (molar percentage) Manganese chloride tetrahydrate respectively was kept in Borosil bottles. Thereafter the mixture was refluxed at 90^0C in a regular laboratory oven for 6 hours for all samples. After that the bottles were eventually allowed to cool down up to room temperature, and the samples were thoroughly rinsed in DI water to dissolve the residual salt and surfactant[24]. Morphological changes in NR samples were investigated by using a field emission scanning electron microscope (FESEM) (Carl-Zeiss). The elemental analysis was carried out in plane-view mode by the energy dispersive x-ray spectroscopy (EDS) system (Oxford Instruments), attached to the FESEM, using 20 kV electron beam. The crystallinity and orientation of ZnO NRs were investigated using X-ray diffraction spectra (Bruker, D8-Discover). The linear optical properties of samples were studied by UV-visible absorption spectroscopy and Photoluminescence (PL) spectroscopy. The variation in absorption-edge of ZnO nanorods due to the introduction of Mn^{2+} ions was estimated from the UV-Visible spectra. The room temperature photoluminescence (PL) spectra were recorded using a FS920 Edinburgh setup using 325 nm, 15mW He-Cd laser as excitation source.

For the nonlinear optical measurements, the experimental set up based on Z- scan technique is shown in the Fig. 1. The single-beam Z-scan experiment was carried out using a Q-switched diode-pumped solid-state (DPSS) laser emitting linearly-polarized, sub-nanosecond pulses in a TEM_{00} mode-intensity profile. The pulse energy varied from 1 μJ to 125 μJ for the measurements with pulse width $t_p \approx$ 0.7 ns at 40 Hz repetition rate so as to minimize the impact of thermally induced optical nonlinearities. The beam was focused to a spot size of $w_0 \approx$ 45μm using a converging lens (f = 150mm) which results in a Rayleigh length ($z_0 = \pi w_0^2/\lambda$) of ≈12 mm. This ensures negligibly small 'sample + substrate' thicknesses compared to z_0. The samples were translated 100 mm distance through beam focal point and the transmitted power in an open-aperture (OA) as well as in a closed-aperture (CA) configuration was measured using fast photo-diode sensor (Model S120C; Thorlabs Inc.).

Results and discussion

Figures 2 (a) – (j) show aqueous grown FESEM micrographs of 0.5, 1.5, 2.0, and 2.5 (mol %) Mn doped ZnO NRs respectively with different magnifications. In all the cases the NRs were grown at 90^0 C temperature for 6 hours. The FESEM micrographs reveal the Mn doping does not affect thehexogonal morphology of ZnO aggregates, because Mn normally substitute the Zn^{2+} sites of ZnO forming $Zn_{1-x}Mn_xO$. The NRs exhibit lengths ranging from ≈ 2 - 4μm with ≈ 400 - 600 nm diameters.

In order to confirm the Mn-doping in ZnO NRs, the EDS spectra were collected from several areas of the samples. The EDS mapping of 1.5% Mn-doped ZnO NRs was recorded from the selected area of the typical electron image as shown in Fig 3 (a). Panels (b)-(d) show the elemental mapping of Zn, O and Mn respectively, which demonstrates the presence of Mn in ZnO NRs. The actual doping of Mn in ZnO NRs were estimated form EDS in terms of atomic % and plotted as a function of molar % of Mn and shown in Fig. 3 (e). From EDS analysis the average atomic % of Mn, calculated from different areas of the samples, were found to be 0.4, 1.2, 1.6, and 1.9 corresponding to 0.5, 1.5, 2.0, and 2.5 % molar concentration of the Mn precursor respectively.

The glancing angle X-ray diffraction pattern of un-doped and 2.5 mol % Mn-doped ZnO NRs are shown in figure 3 (f). The sharp and intense diffraction peak indexed as (002) indicates it's most preferential growth direction and confirms the good crystalline quality for the wurtzite structure of ZnO NRs. This could also be verified from FESEM micrographs where ZnO NRs are erected vertically. After Mn doping the prominent (100), (002), and (101) XRD peaks show shift towards lower theta value as comapared to the undoped NRs, which reveals the development of stress in the matrix due to the expansion in unit cell. The developed stress is primarily a consequence of the substitution of Zn^{+2} ($0.74A^0$) by a larger ionic radii of Mn^{+2} ions ($0.8A^0$). This, again confirms that Mn^{+2} ions have replaced a few Zn^{+2} from the ZnO NR matrix.

Figure 4(a) shows the room temperature (RT) cumulative PL spectra of 0.5%, 1.5%, 2.0% and 2.5% $Zn_{1-x}Mn_xO$ NRs respectively, inset shows the RT PL spectrum of un-doped ZnO NRs. The RT PL spectra show that the Mn-doped ZnO NRs give strong UV emission as a consequence of near-band-edge (NBE) emission and this is

consistent with the bulk ZnO.[25] In addition to NBE emission; there are emission peaks at longer wavelengths due to defect states. PL peaks at 470 nm for all the samples (see Fig. 4(a)) is a distinct signature of defect induced emission. In order to appreciate this feature, we measured the UV-visible absorption spectra of $Zn_{1-x}Mn_xO$ NRs for various Mn-doping concentrations (0.5%, 1.5%, 2.0% and 2.5%) respectively as shown in Fig. 4(b). The absorption spectra for all Mn-doping concentrations (in ZnO NRs) are characterized by peaks around 380-400 nm wavelength (3.26-3.10eV) corresponding to NBE absorptions and there is a discernible asymmetry in each spectrum. The asymmetry in absorption with a long tail extending deeper into the visible band could be understood by noting the existence of closely-spaced multiple defects states close to band-edges which are primarily due to Zn vacancies (V_{Zn}) or O vacancies (V_O). The absorption spectrum of un-doped ZnO NRs markedly differs from the Mn doped spectra (Fig. 4(b)) and it is characterized by appearance of new absorption edges corresponding to the defect states. Using the relation $(\alpha h\vartheta) = \sqrt{[\beta(h\vartheta - E_g)]}$, where α, β, hu and E_g are absorption coefficient, constant, photon energy and band gap respectively, we have converted the absorption spectra into Tauc plot [26] as shown in Fig. 4(c). It has been observed that the band gap of un-doped ZnO NRs is 3.18eV, shown in the inset of figure 4(c). After the Mn-doping has been carried out, the absorption edge begins to appear from lower energy values which supress the bandgap absorption edge. The estimated absorption edge from Tauc plots for $Zn_{1-x}Mn_xO$ NRs are in the range of 2.48 - 2.52 eV shown in figure 4(d). The band gap of Mn doped samples remains same as un-doped ZnO NRs and typical UV emission around 380 nm observed in the PL spectra along with 470 nm peak from defect related states (Fig. 4(a)). Similar observation is also reported by Prabhakar *et al.* [27] for CVD grown Mn doped ZnO NRs. They observed the lower absorption edge of 2.18 eV for 2% Mn doping and explained that the reduced band edge is due to lattice expansion and substitution of Mn ions into the ZnO lattice. We observed the absorption edge at 2. 52 eV for 2% Mn doping whereas 2.53 eV for 0.5% doping. The mismatch in absorption edges reported values[27] may arise due to the method of preparation, experimental parameters, and doping procedure.

It has been observed that the band gap remains almost same with Mn doping concentration. The measured absorption edges of defect states lie substantially close to that for Zn-vacancies or O-vacancies (≈ 2.2 eV) which have been reported earlier.[28] Therefore, a defect induced TPA behavior is expected in such ZnO Nr architectures when irradiated with frequency-doubled near-infrared lasers emitting at 532 nm. Also, the existence of defect states could also bring about enhancement in efficiency of non-resonant nonlinear optical processes.

Figures 5(a-d) and Figures 6(a-d) show representative traces for CA and OA Z-scan measurements for different Mn-doping concentration in ZnO NRs at incident on-axis laser intensity of ≈ 1-3 GW/cm^2.Pre-focal maxima and post-focal minima in the CA transmittance (Figs. 5 a-d) is a signature of self-defocusing effect or a negative value for nonlinear refractive index (n_2). As expected, 0.5% Mn-doped ZnO NRs exhibits a dip in OA transmittance at the focal plane (z=0) in Fig. 6 (a) thereby, indicating a positive value for TPA coefficient (β). However, it is interesting to observe a transmittance peak at the focal plane (z = 0) in OA measurement for higher concentration of Mn-doping in ZnO NRs which can be seen in Fig. 5 (b), (c) and (d). Therefore, enhancement in Mn-doping concentration brings in saturable absorption (SA) characteristics in ZnO NRs which has not been observed before. For comparison, the CA and OA Z-scan transmission of ZnO nanorods at 532 nm are plotted in Fig.7. The pre-focal peak followed by a post-focal variation of CA transmission in Fig. 7 (a) indicates a self-defocusing effect (n_2 is negative). On the other hand, the OA measurement for ZnO nanorods exhibits a drop in transmission at the focal point (see Fig. 7 (b)) which is a distinct signature of positive nonlinear absorption. In order to ascertain the interference of substrate on our NLO measurements, we carried out CA and OA Z-scan transmission of ITO coated quartz substrates at similar laser fluence. We observe that the CA as well as OA normalized transmittance exhibited negligibly weak variation which rules out any contribution from the substrate.

The normalized transmittance for CA (Eq. (1)) and OA (Eq.(2)) Z-scan measurements are given by[23,29]

$$T(z,\Delta\varphi_0) = 1 - \frac{4\Delta\varphi_0 x}{(x^2+9)(x^2+1)} - \frac{2(x^2+3)\Delta\Psi_0}{(x^2+1)(x^2+9)} \quad (1)$$

$$T(z,S=1) = 1 - \frac{\beta I_0 L_{eff}}{2^{3/2}(1+x^2)} \quad (2)$$

Where $x=z/z_0$, $\Delta\varphi_0=kn_2I_oL_{eff}$, $\Delta\psi_0=\beta I_0L_{eff}/2$ are the respective phase changes due to nonlinear refraction and nonlinear absorption, I_0 is the on-axis irradiance at focus (z=0), L_{eff} is effective sample thickness and S=1 corresponds to OA configuration. In order to obtain the macroscopic NLO parameters (n_2 andβ), we theoretically fit the experimental Z-scan traces shown in Fig. 5(a)-(d), 6(a)-(d) and 7((a)-(b)) for different I_0 using Eqs. (1) and (2) respectively. The results are summarized in table-1 for pure ZnO and different Mn-doping concentrations in ZnO NRs. For comparison, we have also tabulated the values of n_2 as well as β for ZnO thin films and un-doped NRs from the available literature[30-33].It is evident that the pure ZnO nanorods as well as Mn-doped ZnO nanorods exhibits self-defocusing effect for all Mn-doping concentrations with at least an order of magnitude higher n_2 values as compared to ZnO thin films. Although, there is a significant degree of inconsistency with regard to the sign of nonlinear absorption (β) of ZnO thin-films, it is apparent that β values for Mn-doped ZnO NRs exhibits significantly higher values in comparison with ZnO thin-films. Such enhancement in n_2 and β could be primarily attributed to Mn-doping as well as geometrical arrangement of Mn-doped ZnO NRs.[34] It is worthwhile to note that the FESEM micrographs in Fig. 2 shows vertically erected Mn doped ZnO NRs with uniform axial dimensions. Even though, the distribution of NRs is random, there exists a Fabry-Perot-like localized resonance due to small-scale ordering within the architecture which results in local enhancement of field[35]. In addition to the creation of defect states (within band gap of ZnO), this local field enhancement leads to increase in NLO interactions and hence, higher values for n_2 andβ.

On a similar note, the variation in NLO characteristics for different Mn-doping concentrations could also be appreciated by analyzing the modifications in band structure as well as geometric arrangement of doped ZnO NRs. The peaks in Z-scan OA transmittance (Figs. 5(b-d)) which indicate a SA behaviour could be attributed to non-availability of unoccupied defect states at high laser intensities. As a consequence, the probability of absorption of incident laser radiation by the population of molecules in ground-state of ZnO NRs (Mn-doping greater than 0.5%) reduces which manifests into transmission maxima at the focal point. In other words, the defect states are close to being completely occupied at high laser intensities (close to focus) and therefore, the ground state absorption reduces.[31,36] This brings about an increase in transmission as we come closer to the focal point. Due to this mechanism, the expected TPA behaviour of Mn-doped (>0.5%) ZnO NRs is completely suppressed and taken over by a feature which characterizes SA behaviour. This point could be substantiated by noting the fact that the charge carriers are trapped more efficiently for higher concentration of Mn^{2+} ions at defect sites which results in elongated lifetime for the defect states.[37,38]Therefore, the defect state population rapidly saturates at high laser intensities for higher concentration of Mn-doping in ZNO NRs. It is also worthwhile to observe that OA normalized transmittance in Fig. 5(a) shows a drop close to focal point (z=0) which is a distinct signature of TPA in 0.5%Mn-doping concentration in ZnO NRs. A plausible reason could be ascertained by observing the fact that the energy of two-photons at 532 nm is 4.67 eV which is almost 1.9 (≈2) times the difference between the ground-state and the defect-state in case of 0.5% Mn-doped ZnO nanorods. Assuming band-to-band transition takes place via simultaneous absorption of two-photons, the defect-state essentially mediates the transition from lower energy band to higher band. In addition, the relaxation lifetimes from defect-state to ground-state are smaller for lower Mn-doping concentrations. This reduces the possibility of saturation for the defect state and enhances the probability of absorption of photons at higher intensities. Therefore, TPA behaviour is expected which is actually being observed is Figs. 6(a) and 7(b).

Conclusions

In conclusion, Mn-doped ZnO NRs were prepared by low temperature aqueous growth technique. The effects of Mn-doping on the geometric structural arrangement, band structure and NLO properties were investigated. For studying the NLO characteristics, single-beam Z-scan technique was employed using a sub-nanosecond excitation source at 532 nm. The UV-visible absorption measurements of ZnO NRs showed marginal change in bandgap as a function for Mn-doping concentrations. In NLO measurements, all the samples with varying concentration of Mn-doping exhibited self-defocusing effect with significantly higher n_2 values as compared to ZnO thin films. The significantly large third-order NLO behavior could be appreciated by observing the modifications in geometrical arrangement and band structure of ZnO NRs as a function of Mn-doping. Un-doped ZnO NRs and 0.5% Mn doped ZnO

NRs exhibited TPA features while strong SA behavior was observed for 1.5%, 2%, 2.5% Mn-doping concentration. In addition to difference in NLA response for OA measurements, the magnitude of β for ZnO NRs varies negligibly as Mn-doping concentration in ZnO NRs change. From this investigation, it could be suggested that Mn-doping in ZnO NR architecture facilitate improved NLO interactions which can be employed for designing ultrafast photonic switches and efficient optical phase-shifters. The MPA observed in pure ZnO NRs and 0.5 % Mn doped ZnO NRs suggest their utility in nonlinear optical devices such as optical limiters while higher Mn-doped ZnO NRs could be a suitable candidate for saturable absorber materials.

Acknowledgements

The authors acknowledge the funding from National Institute of Science Education and Research (NISER), Department of Atomic Energy (DAE), India.

References

1 Z. L. Wang, J. Phys.: Condens. Matter , 2004, **16**, R829-R858.

2 H.Morkoc and U.Ozgur, Zinc Oxide: Fundamentals, materials and device technology 2009, WILEY-VCH Verlag GmbH & Co. KGaA, Weinheim.

3 A. B. Djurisic and Y. H. Leung, Small, 2006, **2**, 944-961.

4 M. H. Koch, P. Y. Timbrell and R. N. Lamb, Semicond. Sci. Technol., 1995, **10**, 1523-1527.

5 Y. W. Zhu, H. Z. Zhang, X. C. Sun, S. Q. Feng, J. Xu, Q. Zhao, B. Xiang, R. M. Wang and D. P. Yua, Appl. Phys. Lett., 2003, **83**, 144-146.

6 C. J.Lee, T. J. lee, S.C. Lyu, Y Zhang, H. Ruh and H. J. Lee, Appl. Phys. Lett., 2002, **81**, 3648-3650**.**

7 T. Gao and T.H. Wang Appl. Phys. A, 2005, **80**, 1451-1454.

8 Z.L.Wang and J. Song, *Science ,* 2006, **312**, 242-246.

9 Z. Fan, D. Dutta, C. J. Chien, H. Y. Chen, E. C. Brown, P. C. Chang, and J. G. Lu, Appl. Phys. Lett., 2006, **89**, 213110.

10 Y. C. Kong, D. P. Yu, B. Zhang, W. fang and S. Q. Feng, Appl. Phys. Lett., 2001, **78**, 407-409**.**

11 B. F. Levine, Phys. Rev. Lett., 1970, **25**, 440-443.

12 W.Rong-yao, W. Xiao-chun, Z. Bing-suo, W. Li, W.Peng-fei, L. Shao-mei, W. Jin-guo and X.Ji-ren, Chinese Phys. Lett., 1998, **15**, 27-29.

13 R. Prasanth, L. K. van Vugt, D. A. M. Vanmaekelbergh and H. C. Gerritsen, Appl. Phys. Lett., 2006, **88**, 181501.

14 B. E. Sernelius, K.-F.Berggren, Z.-C.Jin, I. Hamberg and C. G. Granqvist, Phys. Rev. B, 1988, **37,**10244.

15 A. G. Ali, F. B. Dejene and H. C. Swart. Cent.Eur. J. Phys., 2012, **10(2)**, 478-484.

16 M. H. Huang, S. Mao, H. Feick, H. Yan, Y. Wu, H. Kind, E. Weber, R. Russo and P. Yang, Science, 2001, **292**, 1897-1899.

17 R. Konenkamp, R. C. Word, and C. Schlegel, Appl. Phys. Lett.,2004, **85**, 6004-6006.

18Y. S. Wang, P. J. Thomas, and P. O'Brien, J. Phys. Chem. B, 2006, **110**, 21412-21415.

19R. K. Sharma, S. Patel and K. C. Pargaien. Adv. Nat. Sci.: Nanosci Nanotechnoly, 2012, **3**, 035005 .

20 D. C. Kundaliya, S. B. Ogale, S. E. Lofland, S. Dhar, C. J. Metting, S. R. Shinde, Z. Ma, B. Varughese, K. V. Ramanujachary, L. Salamanca-Riba, and T. Venkatesan, Nat. Mater., 2004, **3**, 709-714.

21 J. S. Miller and M.Drillon, Magnetism: Molecules to materials V, 2005,WILEY-VCH Verlag GmbH & Co. KGaA, Weinheim, p.p. 43-44.

22 J. B. Cui, C. P. Daghlian, U. J. Gibson, R. Pusche, P.Geithner and L. Ley, J. Appl. Phys., 2005, **97**, 0443151.

23 M. Sheik-Bahae, A. A. Said and T.-H. Wei and D. J. Hagan and EW Van, IEEE J. Quantum Electron, 1990, **26**, 760-769.

24 B. Panigrahy, M. Aslam, and D. Bahadur J. Phys. Chem. C 2010**, 114**, 11758–11763.

25 V. A. Fonoberov, K. A. Alim, and A. A. Balandin, Phys. Rev. B, 2006, **73**, 165317.

26 J. I. Pankove, Optical Processes in Semiconductors, 1971, Prentice-Hall Inc., Englewoord Cliffs, NJ.

27 R. R. Prabhakar, N. Mathews, K. B. Jinesh, K. R. G. Karthik, S. S. Pramana, B. Varghese, C. H. Sow and S. Mhaisalkar J. Mater. Chem., 2012, **22**, 9673-9683.

28 C. Johnson, K. Kittilstved, T. Kaspar, T. Droubay, S. Chambers, G. Salley and D. Gamelin, Phys. Rev. B, 2010, **82**,115202.

29 M. Yin,H. Li, S. H. Tang and W. Ji,Appl. Phys. B, 2000, **70**, 587-591.

30 X. Zhang, H. Fang, S. Tang, W. J, Appl. Phys B Laser and Optics, 1997, **65**, 549-554.

31 J.H. Lin, Y.J. Chen, H.Y. Lin and W. Hsieh , J. Appl. Phys., 2005, **97**, 033526.

32 H. W. Lee, K. M. Lee, S Lee, K. H.Koh, J. Y. Park, K. Kim and F.Rotermund Chem. Phys.Lett., 2007, **447**, 86-90.

33 S.K. Min, C.-H. Oh, G. J. Lee , Y. P. Lee ,S.K. Min and S.H. Han, J. Korean Phys. Soc., 2009, **55**, 1005-1008.

34 C. Torres-Torres, M. Trejo-Valdez, H. Sobral, P. Santiago-Jacinto and J. A. Reyes-Esqueda, Phys. Chem. C, 2009, **113**,13515-13521.

35 S. Arab, P. D. Anderson, M. Yao, C. Zhou,P. D.Dapkus,M. L. Povinelli and S.B. Cronin, Nano Res., 2014, **7(8)**, 1146-1153.

36 Y.P. Chan, J.-H. Lin, C. C. Hsu and W.-F. Hsieh, Opt. Express, 2008, **16**, 19900-19908.

37 R.Podila, B. Anand, J.T. Spear, P. Puneet, R. Philip, S.S.S.Sai, A.M.Rao, Nanoscale, 2012, **4**, 1770-1775.

38 A. Layek, B. Manna and A. Chowdhury, Chem. Phys. Lett., 2012,**539**, 133-138.

Figure captions

Figure1. Schematic of the Z scan experimental set up. HWP: Half wave plate, PBS: Polarizing beam splitter, L: Lens (150mm), S: Sample, A: Aperture, PD1: Reference detector, PD2: Signal photo detector.

Figure2. Panels (a),(c),(e), and (g) show the FESEM micrographs of 0.5%,1.5%,2%, and 2.5% Mn-doped ZnO NRs respectively and panel (b), (d), (f), and (h) show the magnified view of panels (a), (c), (e), and (g), respectively.

Figure 3. (a) FESEM image of Mn doped ZnO NRs, (b)-(d) EDS elemental maped images of Zn, O and Mn respectively, (e) Calculated atomic percentage of Mn K_α edge with respect to the molar percentage of Mn in the solution (f) X-Ray diffraction pattern of Pure ZnO NRs and Mn doped ZnO NRs on ITO (*) substrate respectively, the inset show magnified view of (100), (002), and (101) phases of ZnO and Mn Doped ZnO NRs.

Figure4. (a) Room temperature (RT) photoluminescence spectra for various doping of $Zn_{1-x}Mn_xO$ ZnO NRs, RT PL spectrum of ZnO NRs shown in inset (b) RT absorption spectra of pure ZnO NRs and $Zn_{1-x}Mn_xO$ NRs (c) Tauc Plots of $Zn_{1-x}Mn_xO$ NRs, ZnO NRs shown in inset and (d) Band gap calculated from (c) of $Zn_{1-x}Mn_xO$ NRs as a function of Mn doping concentrations.

Figure5. Closed aperture (CA) *Z*-scan curves for $Zn_{1-x}Mn_xO$ nanorods for different Mn-doping concentration (a) $x = 0.005$ (b) $x = 0.015$ (c) $x = 0.02$ and (d) $x = 0.025$

Figure6. The open aperture (OA) Z-scan curves for $Zn_{1-x}Mn_xO$ nanorods for different Mn-doping concentration (a) $x = 0.005$ (b) $x = 0.015$ (c) $x = 0.02$ and (d) $x = 0.025$

Figure7. (a) Closed Aperture (CA) and (b) Open Aperture (OA) Z-scan traces for Pure ZnO nanorods

TABLE I. Summary of NLO properties of ZnO thin films and ZnO Nanorods

Sample	$n_2(cm^2/W)$	$\beta(cm/W)$	Parameters	References
ZnO thin films	-0.90×10^{-14}	4.20×10^{-9}	λ=532nm; Pulse width=25 ps	[30]ref.
ZnO thin films	2.57×10^{-11}	-1.53×10^{-7}	λ=830nm; Pulse width=175fs	[31]ref.
ZnO nanorods	3.11×10^{-10}	5.61×10^{-6}	λ=815nm; Pulse width=85fs	[32]ref.
ZnO thin films	5.57×10^{-11}	-0.61×10^{-6}	λ=815nm; Pulse width =85fs	[32]ref.
ZnO nanorods	–	5.90×10^{-7}	λ=800nm; Pulse width = 130fs	[33]ref
ZnO nanorods	2.1×10^{-10}	3.5×10^{-5}	λ=532 nm; Pulse width = 0.7 ns	This work
0.5%Mn doped ZnO	-1.88×10^{-10}	1.32×10^{-5}	λ=532nm ; Pulse width	This work

nanorods			=0.7ns	
1.5% Mn doped ZnO nanorods	-1.59×10^{-10}	-1.03×10^{-5}	λ=532nm ; Pulse width =0.7ns	This work
2% Mn doped ZnO nanorods	-1.25×10^{-10}	-4.17×10^{-6}	λ= 532 nm; Pulse width =0.7ns	This work
2.5% Mn doped ZnO Nanorods	-1.34×10^{-10}	-5.45×10^{-6}	λ=532nm ; Pulse width =0.7ns	This work

Figure 1 Singh et al.

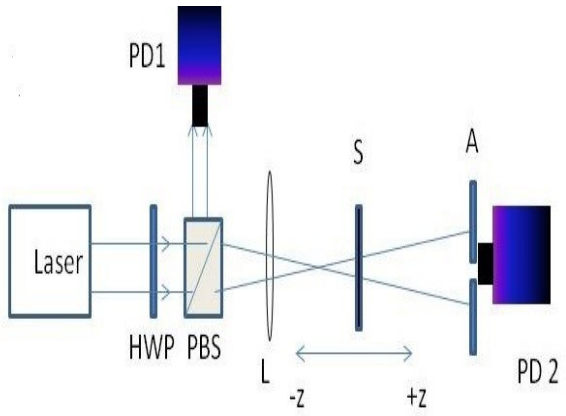

Figure 2 Singh et al.

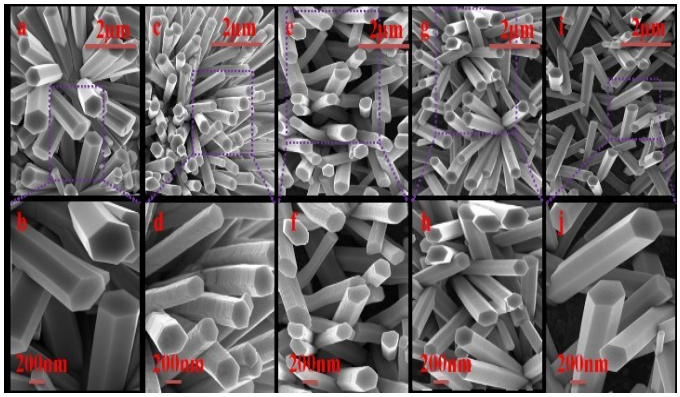

Figure 3 Singh et al.

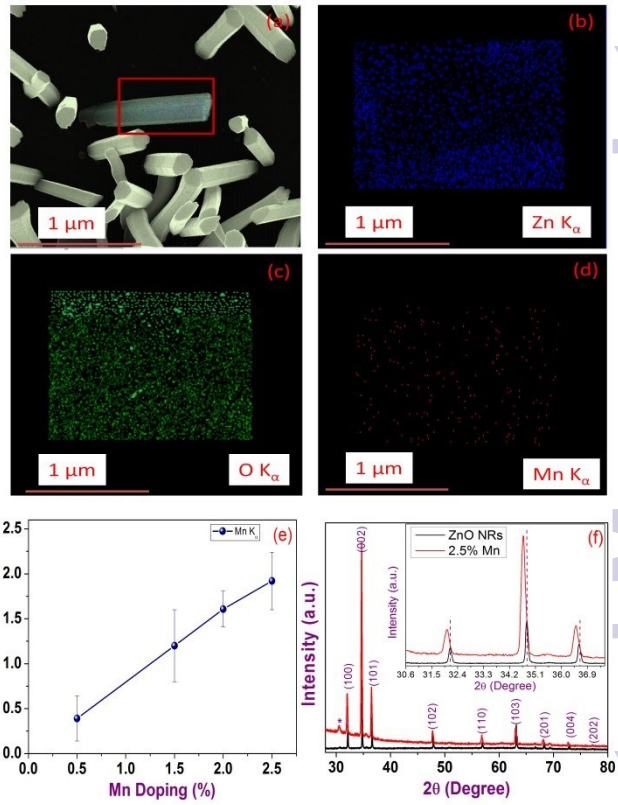

Figure 4 Singh et al.

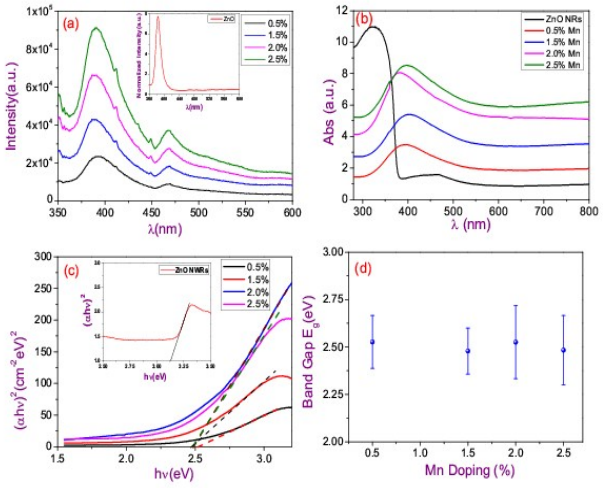

Figure 5 Singh et al.

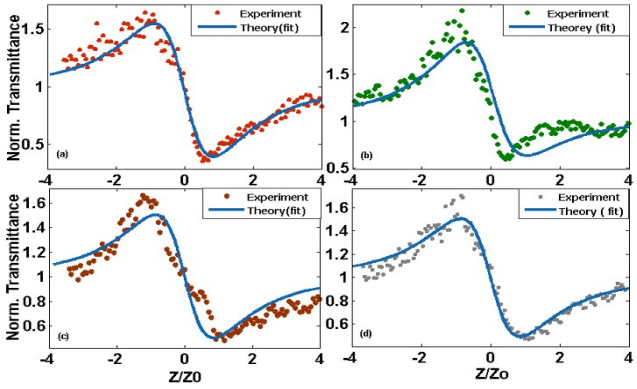

Figure 6 Singh et al.

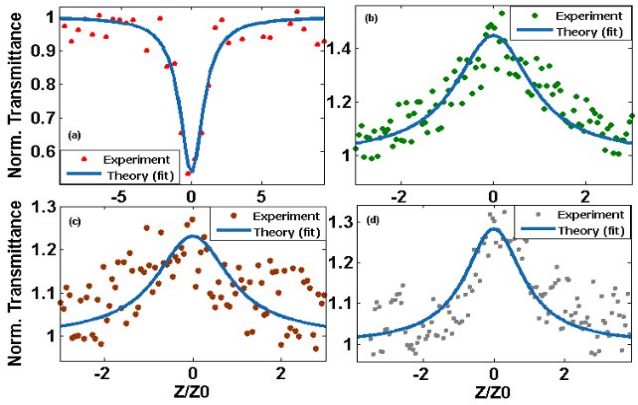

Figure 7 Singh et al.